

Preliminary Study of the Feasibility of a Non Crystalline Positron Emission Tomography Using a Suspension of Superheated Superconducting Grains (SSG) in High Density Dielectric Matrix (HDDM) as Detector

Roger Bruère Dawson ^{a,b}, Jacques Maillard ^{b,c},
G rard Maurel ^d, Jorge Silva ^e, Georges Waysand ^a

^a*GPS UMR 7588, Universities Paris VI and Paris VII, 4 place Jussieu, 75005 Paris France*

^b*IN2P3, 3 rue Michel Ange, 75794 Paris Cedex 16*

^c*CNRS IDRIS, Bt 506, BP167 91403 Orsay Cedex France*

^d*CHU Hopital Saint Antoine, Paris VI, Facult  de M decine, 27 rue de Chaligny 75012 Paris France*

^e*Universit  Paris VI, 4 place Jussieu, 75005, Paris, France*

Abstract

Suspensions of superheated superconducting grains are a detecting composite material. Each grain in the suspension is a microcalorimeter with an energy threshold defined by its equatorial magnetic field for a given temperature. The higher the matrix density, the larger the gamma stopping power. For several years, cylindrical cells of such suspensions about 2 cm long and 0.4 mm in diameter can be read out in real time. As a result, using two independent cells, one can record a time coincidence between them. This could be potentially very useful for positron cameras where two diametrically opposite cells are simultaneously knocked by 511 keV gammas. This paper, based on the state of art in SSG in high density matrix, discusses such a feasibility.

Key words: Nuclear Medicine; Monte-Carlo Simulation; Micro PET; Detector; Superconductivity.

Email address: maillard@idris.fr (Jacques Maillard).

1 Positron Emission Tomography (PET) and Suspensions of Superheated Superconducting Grains in High Density Matrix

Superheated superconducting grains detectors (SSG) are made from a suspension of microspheres of type I superconductor. Kept at a temperature lower than the superconducting critical one and in a DC magnetic field larger than the thermodynamical critical value at that temperature, each grain remains in a superconducting state, which is indeed a superheated superconducting state (this is not valid for a bulk superconductor because of surface defects acting as permanent nucleation centers). This superheated state can be broken down, either by ramping up the magnetic field, or by heating the microsphere (by energy deposition). In both cases, the perfect diamagnetism associated with the superconducting state disappears suddenly. The resulting local magnetic flux variation can be detected in real time by a pick-up coil surrounding the whole suspension. Although good type I superconductors are : Al, Zn, Ga, Ge, Cd, In, Sn, Hg, Tl, the most commonly used metal is tin because of its characteristic values for the superconducting state: $T_c = 3.72\text{K}$ just below the 4, 2K for liquid helium under atmospheric pressure, $H_c(0)$ (at zero K) =302 Gauss $H_{sh}(0) =600$ Gauss. Low temperature techniques are no more a problem in medical environment: MRI magnets are immersed in tens of litres of liquid helium and on the other hand pulse tube system can provide liquid helium in closed loop systems. Non toxicity and friendly metallurgy of microspheres are secondary reasons for that choice. Usually the microspheres are randomly but homogeneously dispersed in paraffin wax (reference [1]). As a result such a suspension has a low stopping power for 511 keV gamma since the filling factor in tin grains cannot be larger than 0.1 to avoid percolation between grains. For positron camera, it is possible to replace wax by litharge (PbO), the composite of tin grains and PbO is therefore a suspension of SSG in High Density Dielectric Matrix (HDDM). Because of the presence of high Z element in such a composite one has to take into account not only the ionization process but also the photoelectric effect under 511 keV irradiation. In recent years the sensitivity of the sudden flux change read-out has been enhanced with the use of a preamplifier with an HEMFET input stage (reference [2]) cooled in liquid helium. We assume throughout this paper that the sensitivity of the preamplifier is high enough to read a single grain larger than $10\mu\text{m}$ in diameter in the pixel defined below or in an equivalent volume. For the following :

- 1- We recall the basics physics of SSG.
- 2- We describe the detecting system with SSG-HDDM, with its main parameters, technical limitations and constraints limiting ourselves to a single cell of the previous system.
- 3- Using GEANT (reference [3]) simulation program we study its behavior under 511keV irradiation. These results allow us to estimate the read-out

performance under positron irradiation.

4- Finally we discuss the requirements for a completion of such a system.

2 Basic Physics and Geometry of the elementary pixel of a Positron Camera with HDDM-SSG

2.1 Basic physics

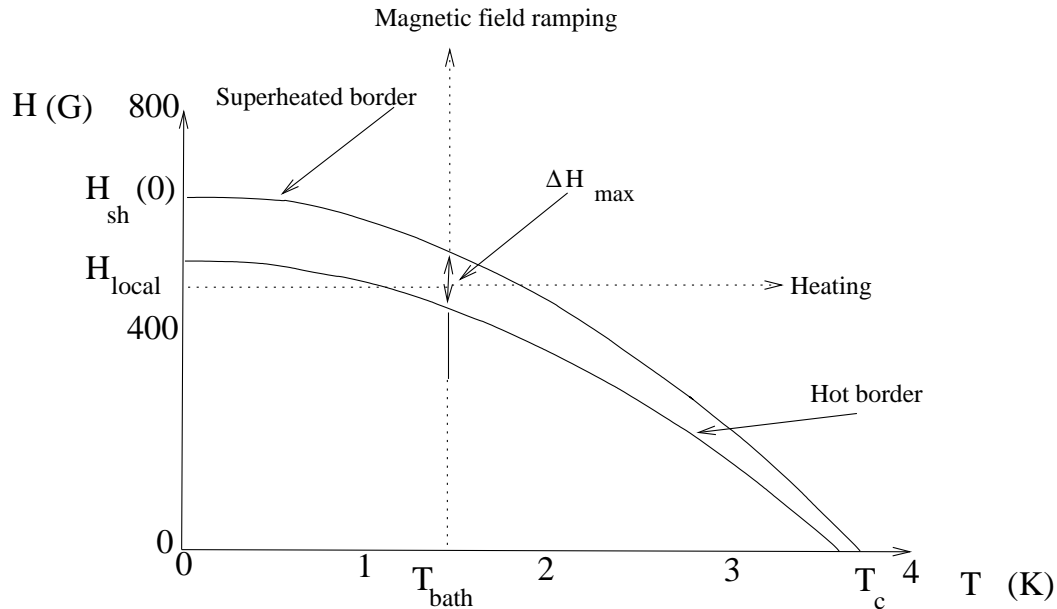


Fig. 1. Phase diagram

In a phase diagram (T, H) (reference [4] page 2, see figure1) one grain of the suspension can be represented by one point (H_{local}, T_{bath}). T_{bath} is the bath temperature in which the suspension is immersed. H_{local} is the value of the magnetic field at the equator of the grain or its surface maximum if the grain is not perfectly spherical. H_{local} is different from $H_{applied}$ because of diamagnetic interactions between grains. Diamagnetism is the magnetic field expulsion from the volume of the superconducting material (here the grain), as a result from grain to grain there are field variations induced by these magnetic flux expulsions. Therefore in the phase diagram a suspension of grains at a given temperature T_{bath} is represented by a set of points along the vertical line $T=T_{bath}$. If these grains are numerous, the suspension can be represented by a vertical segment : each point of this segment represents one grain and only one. There are two main paths for a grain to undergo a change of state : either by heating or by magnetic field ramping up. Heating can be produced by energy deposition, if enough energy is deposited one has a thermal nucleation mechanism. In the case of magnetic field ramping up one

speaks of magnetic nucleation. It is the distance from the representative point in the phase diagram to the superheated border which defines the amount of energy necessary for thermal nucleation. It has been demonstrated that the heating of a superheated grain under energy deposition is, after a very short time, (10^{-10} - 10^{-12} second), homogeneous.

In principle, since the diamagnetic interactions between microspheres are long range interactions, each transition of a microsphere to the normal (resistive state) modifies the magnetic field sensed by each grain of the suspension. However, if only a small fraction of the grains undergo a transition one can safely consider in first approximation that these modifications are negligible. It is only when a large fraction of the grains have changed state that one must take into account the modification of diamagnetic interactions. This problem has been analytically solved by Geigenmüller and Mazur (reference [5]): given the geometrical positions of the remaining superconducting grains, the magnetic field at the equator of each of them is computable (reference [6]). More recently it has been discussed by Peñaranda et al (reference [7]).

2.2 *Geometry of a single pixel*

As a starting point to evaluate which kind of benefit one could expect from such a system as a positron camera, we take the most conservative parameters for the elementary cell :

Geometry: a cylinder 0.78 cm long ; 0.4 cm in diameter

Temperature: about 200mK

Magnetic Field: $H_c(0,2K) = 300$ Gauss, $H_{sh}(0,2K) = 600$ Gauss.

It is assumed that each cell is a suspension with a filling factor of 0.1 for tin microspheres of respectively 7, 8 or $10\mu\text{m}$ diameter. For larger filling factor contacts or quasi contacts between grains create strong diamagnetic interactions resulting in local fields stronger than the theoretical superheated critical magnetic field : the grains are no longer superconducting. The energy loss of the particle being proportional to the radius of the microsphere of the trajectory, and the heating of the microsphere proportional to the inverse of the cubic of radius, the heating decreases inversely to the square of the radius. The energy thresholds decrease with the radius of the microsphere.

Due to the modularity of the system, we can take one of these cells to simulate the behaviour under 511 keV irradiation of the full detector. Our tool for simulation is GEANT 321 (reference [3]). This program takes into account all the possible interactions of an impinging photon on the cell: ionisation and radiation including secondary effects. It is a step by step simulation: the trajectory of the particle is incremented step by step in a minute quantity

depending on one hand on the particle nature, lifetime and momentum, and on the other hand on the crossed media (chemical composition, density and surrounding boundaries). To simulate the whole pixel needs too much memory space, therefore we consider a fraction of it along the irradiation axis and a diameter of 0.1 cm. GEANT is unable to deal at once with such a large number of grains; therefore, along the axis we divide the cylinder into sub cylinders. The final simulation represents a volume of 8 mm³. In GEANT one is free to choose the minimum step: it has been taken here as a fraction of a micrometer. For each step GEANT gives the energy loss in that step, the eventual gamma interaction, the deposited energy per grain and finally the number of crossed granules with energy deposition.

3 Deposited energies in the suspension

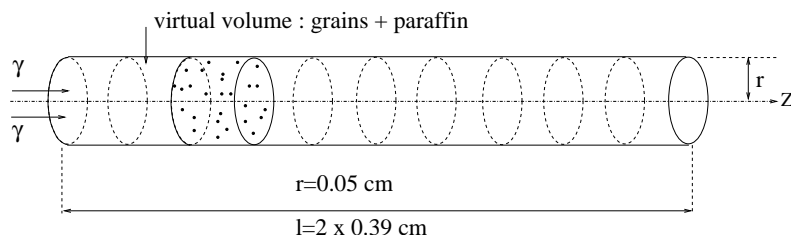


Fig. 2. Geometry of simulation

The gamma beam is parallel to the cylinder axis, arbitrarily chosen as the Z axis (2). 10^5 photons are sent onto the detector which is a suspension of mono-sized tin microspheres either 7, 8, or 10 μm in diameter, representing 10% of the volume cylinder. The microspheres are immersed in a high density matrix made of litharge (PbO, density =9.35). Such a detector irradiated by 511keV gammas has a stopping power of about 37% : Simulation gives that out of 100 000 photons impinging on the cylinder, 36713 interact by electron production either by Compton or by photoelectric effect. As we will see the energy deposition in both processes occurs in the vicinity of the spot of materialisation of the impinging photon.

3.1 Distribution of the interaction points:

Figure 3 represents the projections (X and Y) on a diametrical plane of the interaction spot of each interacting gamma in the whole cylinder. The aperture of the gamma beam is reduced to 10 μm around the Z axis. In this representation one does not care if the interaction takes place in a microsphere or in the matrix. One can see that the diameter of the virtual volume is large enough to include all the diffused events.

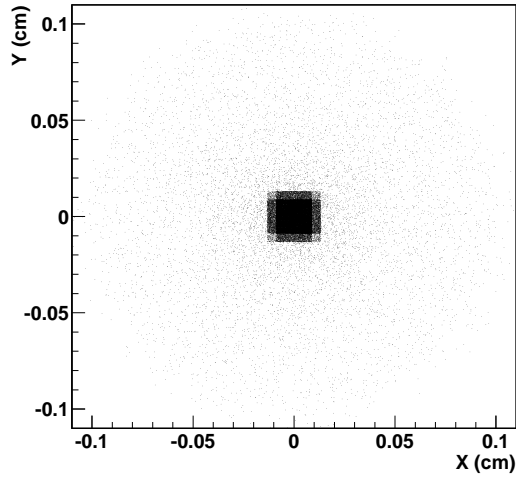


Fig. 3. xy projection of γ impact: its dispersion is one order of magnitude smaller than the radius of the simulated cylinder

3.2 Distribution of crossed microspheres :

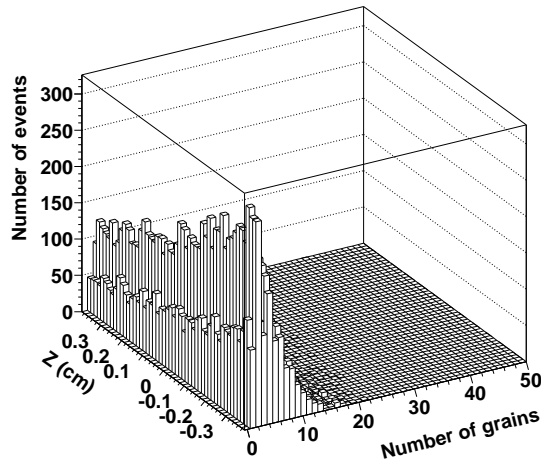


Fig. 4. Number of crossed grains versus the depth Z: the number of grains does not depend of Z

As long as the photon does not interact with the pixel there is no energy deposition. This deposition takes place only along the secondary trajectories. The energy loss useful for read-out of a photon impact occurs only in the grains. We reserve the denomination "crossed grains" or "crossed microspheres" to these specific microspheres in which there is an energy deposition. Figure 4 represents the number of crossed grains per incoming photon as a function of the depth Z in the cylinder. As expected, since the mean free path of electrons is shorter than the mean free path for photons one can see that the number of crossed granules is depth independent of the photon impact. As a result, the

energy loss after a photon interaction is independent of the point where it has occurred.

3.3 *Distribution of crossed grains with energy of gamma:*

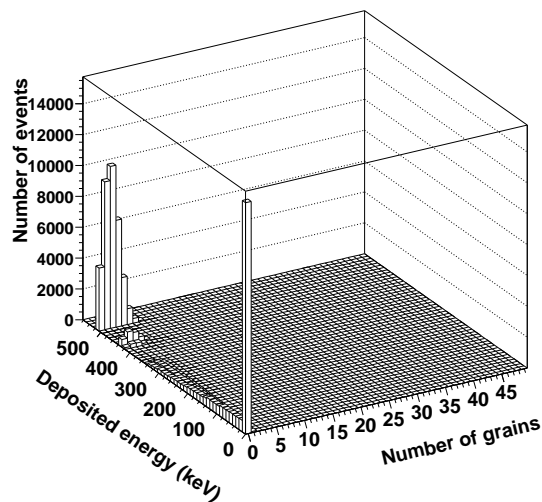


Fig. 5. Number of grains hit versus the whole energy deposition in the cell (in the litharge and in the grains)

This distribution is represented in figure 5 which gives the fraction of concerned grains for a given range of deposited energy by an impinging electron. At this stage we have a full description of the deposited energies in the suspension. So far we have not used the superconducting state properties. Now we have to estimate the response of the superheated superconducting system to this distribution of deposited energy.

3.4 *Response of superheated superconducting microspheres to an energy deposition*

For the purpose of the feasibility study it is enough to limit ourselves to a small number of crossed grains thus representing a tiny fraction of their overall number. In principle, for each change of state of a grain, because of the long range diamagnetic interaction, the whole set of maxima of the equatorial magnetic field is changed. However, when only a small number of grains are undergoing a transition one can assume that the distribution of maxima of the equatorial magnetic field remains the same.

As a result the simulation relies on two quantities which, in first approximation are taken as independent stochastic phenomena:

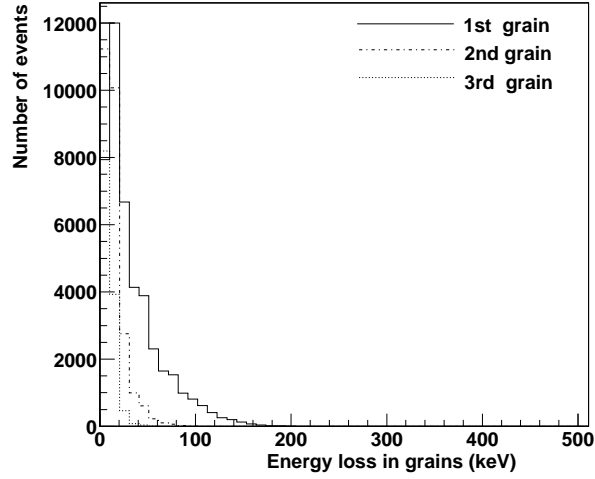


Fig. 6. Energy loss in the grains: the grains are ordered by the amount of deposited energy, the first one is represented by the continuous line

- the energy of the gamma when entering into the grain.
- the equatorial magnetic field on the corresponding grain.

(the impact point is not a relevant parameter because the energy deposition if large enough always creates an homogeneous nucleation : there is a uniform and global heating of each flipped grain (flipped = crossed grains that will change state)). In other terms the distribution of deposited energies among crossed grains is convoluted with the distribution of their equatorial magnetic field.

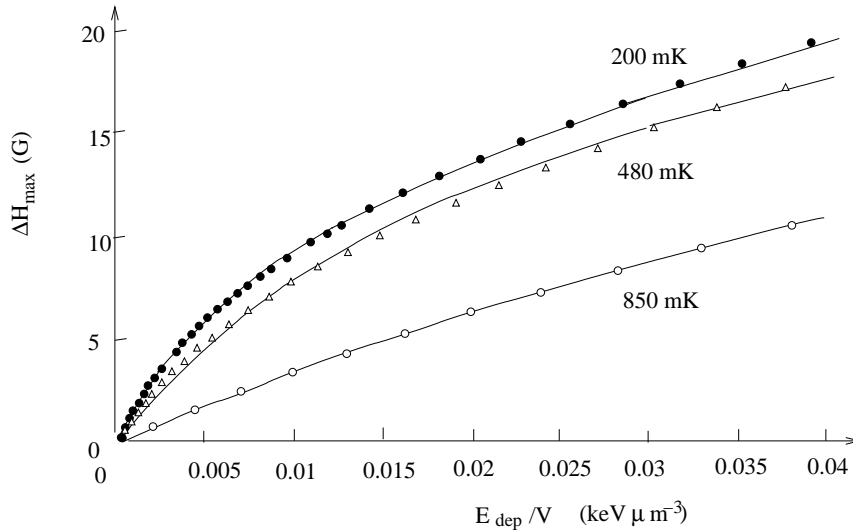


Fig. 7. Energy deposition in the grains versus ΔH_{max} . Incidentally for each T_{bath} this gives the correspondence between ΔH in gauss and “ ΔH ” in eV.

Figure 7 (reference [4] page 82) shows the ΔH_{max} in function of the density of energy deposition in the grain, for three different temperatures. If we multiply

this density by the volume of the microsphere (the grain) we get for a given temperature, and a certain energy deposition, the range of ΔH , that we can randomly choose between 0 and ΔH_{max} .

Thus we obtain as a function of the impinging photon energy the intrinsic efficiency of the pixel (figures 8,9 and 10) assuming that at H applied 20% of the grains are already flipped to the normal state and that in the interval $[H_{applied}, H_{applied}+\Delta H_{max}]$ the number of grains per unit of ΔH is constant.

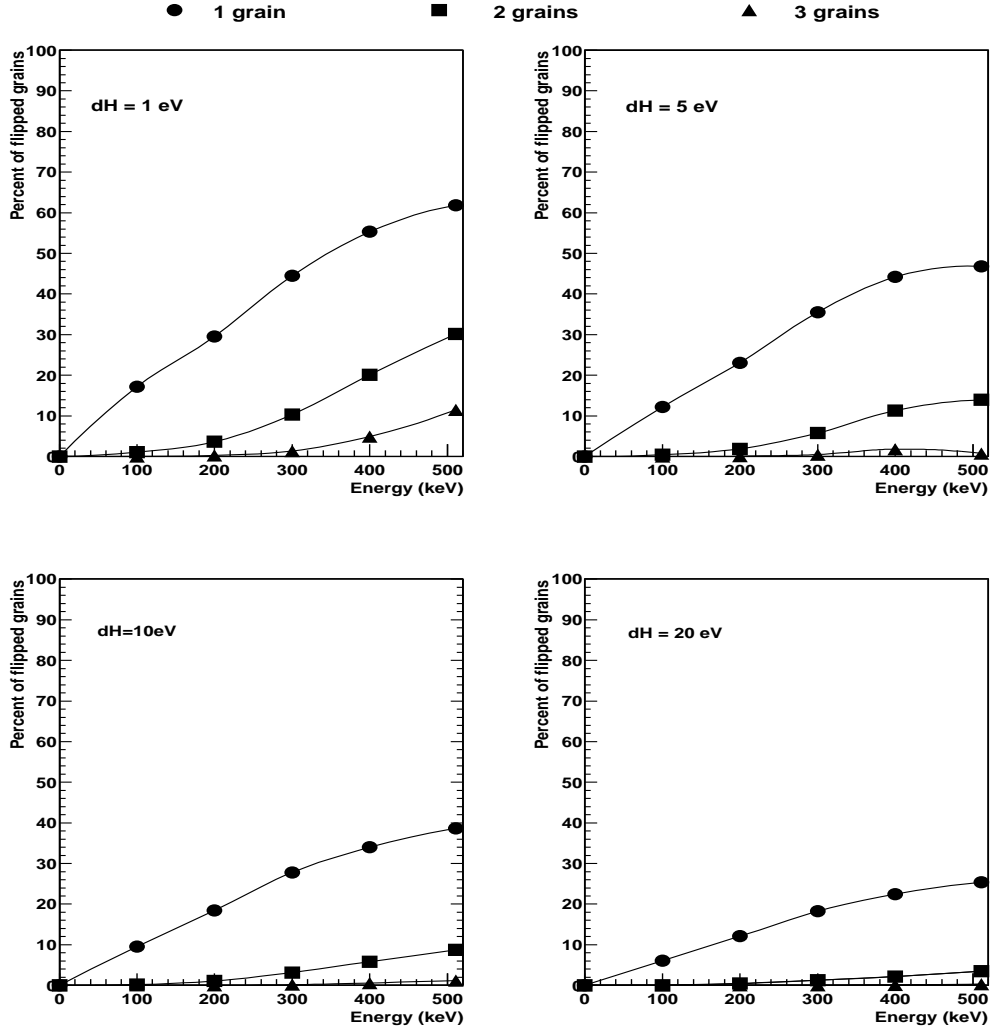


Fig. 8. Photon electronic detection efficiency in function of energy, for grains with 10 micron of radius

In fact, on figures 8, 9 and 10 for a given suspension three efficiencies have been drawn as a function of the impinging gamma respectively corresponding to the simultaneous flipping of 1, 2 or 3 grains. 3 different radius of grains has been used, $10\mu\text{m}$, $8\mu\text{m}$, $7\mu\text{m}$. Four different ΔH were used, 1 eV, 5 eV, 10 eV, and 20 eV per μm^3 . As expected the resulting curves are strikingly different and lead us to consider that the event selection can be based not only on energy

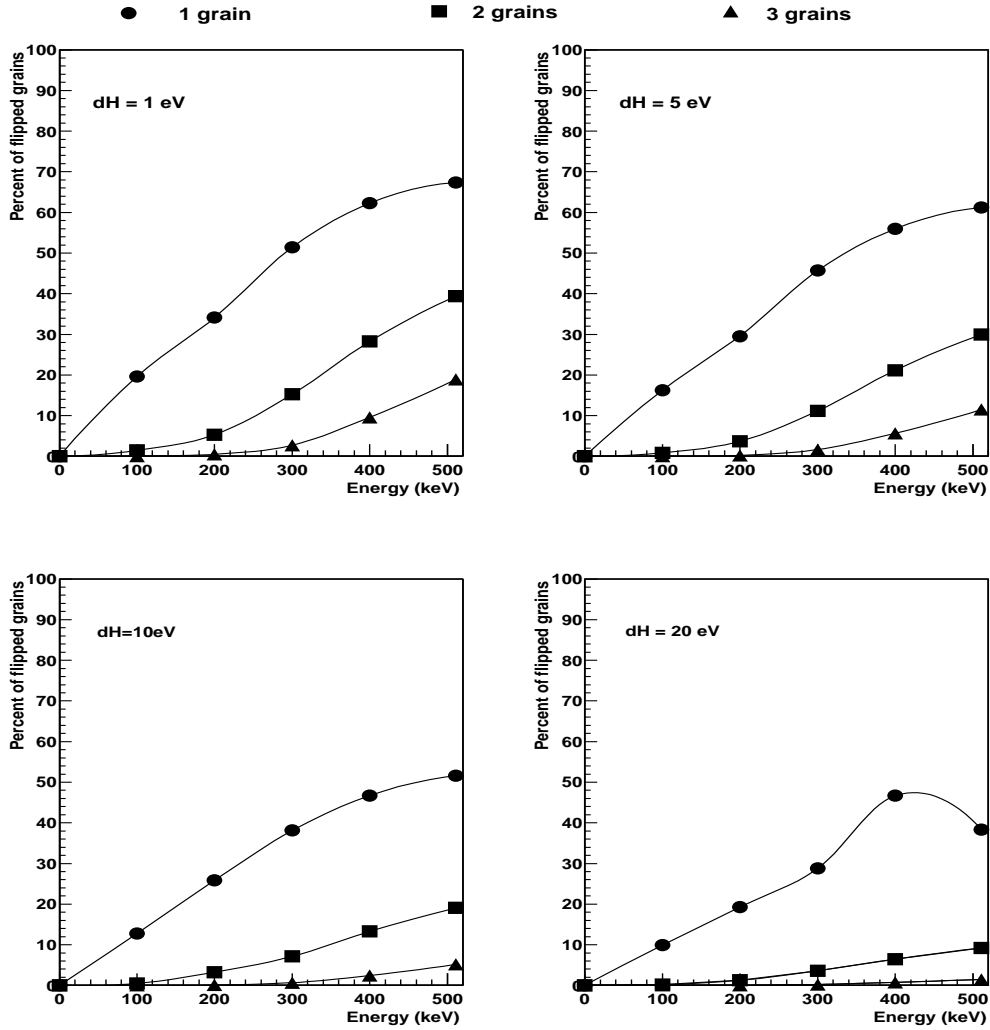


Fig. 9. Photon electronic detection efficiency in function of energy, for grains with 8 micron of radius

selection by magnetic field monitoring which is conventional in SSG systems but, in that case can be combined with signal amplitude selection. This opens a wide range of configuration for PET. To appreciate the potentialities of a SSG PET let us consider the classical case of a small animal camera. The present state of art of the electronic read-out allows us to read 1 grain of 10 μm radius or 2 grains of 8 μm radius. 5 eV of ΔH is assumed. ΔH_{max} of 5 eV per cubic micron is a good compromise, allowing to work with reasonable temperature (between 200 and 500 mK, see figure 7) and precision (5 keV per μm^3) correspond to an energy loss of 20 keV in grain of 10 μm radius, see figure 6). We can for example estimate the electronic efficiency of the system at 511 keV:

- for 10 μm : 0.534
- for 8 μm : 0.380

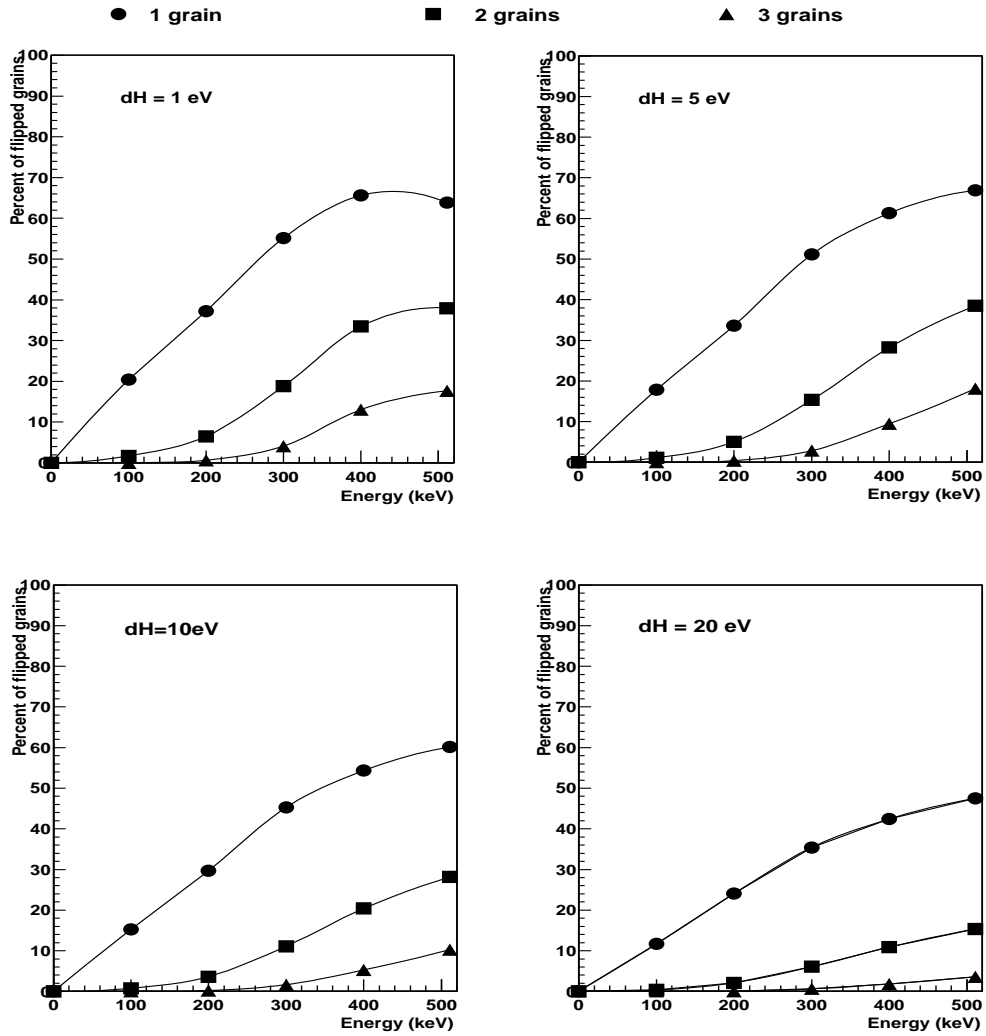


Fig. 10. Photon electronic detection efficiency in function of energy, for grains with 7 micron of radius

A more sophisticated simulation shall mix the different radii of grains, allowing more subtle energy differentiation.

4 Performance required for a small animal PET

The PET requirements were discussed among others by Huber et al ([8]). One considers a mouse phantom of 29g placed in the centre of a 20 cm long cylinder, 5 cm in diameter made of two closed compact layers of elementary cylindrical pixels as discussed above (see figure 11).

Monte Carlo simulation gives a materialization efficiency (Table 1) to 511 Kev irradiation of the order of 42% in a pixel. This efficiency can be higher if one

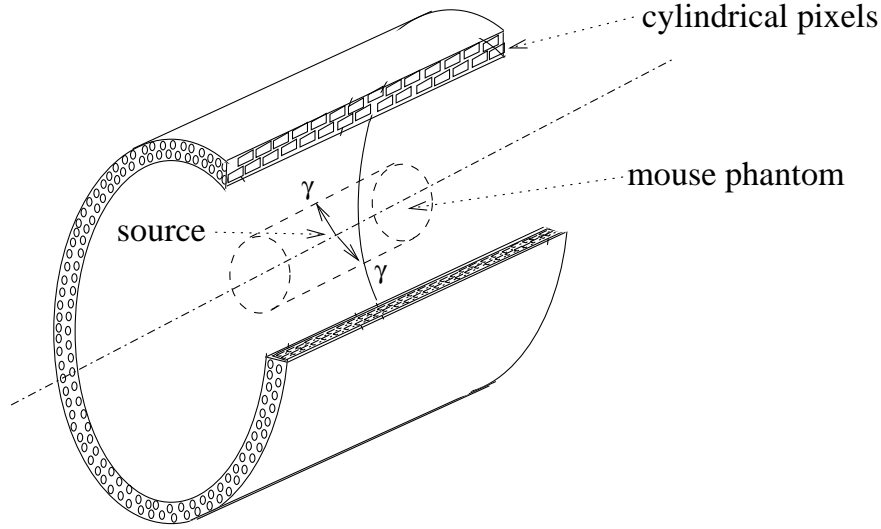


Fig. 11. Micro PET geometry

increases the depth of the detecting layer. This is possible because, contrary to classical techniques neither the read-out electronics nor the detecting material are limiting factors for an efficient design of the whole system.

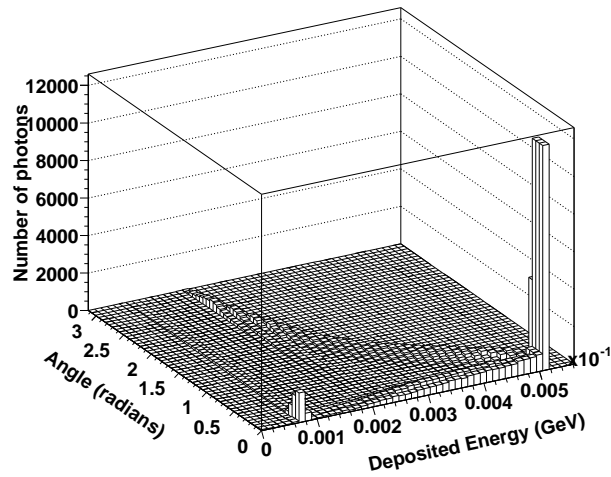


Fig. 12. Deposited energy in the cell for straight and diffused photons, versus the angle between the emitted photon and the hitted cell

The energy deposited in the pixel comes from either a straight gamma (signal) or from a diffused trajectory in the mouse phantom (noise). Figure 12 gives the distribution of the deposited energy for the straights and the diffused photons. The efficiency given by fig 7 allows an estimation of the noise equivalent counting rate (NECR) which is the ratio of interest for PET performances. For its estimation we follow conventional notations. The true (*True*) coincidental and scatter (*Scatter*) rates are given by, μ being a constant,

$$True = \mu \cdot \rho \cdot (\epsilon^2) \cdot g_t \cdot (P^2)$$

and

$$Scatter = f_s \cdot True$$

respectively, where

ρ is the activity density,

ϵ is the single detection efficiency,

g_t is a geometry efficiency for true coincidence events,

P is the probability for escape for a 511 keV photon from the small animal,

f_s is the scatter fraction.

The random (*Random*) coincidence event rate is proportional to single event rate (*Single*)

$$2 \cdot \tau \cdot (Single)^2$$

where

$$Single = \rho \cdot \epsilon \cdot g_r \cdot P$$

that means:

$$Random = \mu \cdot 2 \cdot \tau \cdot \rho^2 \cdot \epsilon^2 \cdot g_r^2 \cdot P^2$$

and

$$Random = True \cdot \rho \cdot g_t \cdot 2 \cdot \tau$$

where

τ is the coincidence resolving time (usually 10 or 5 ns)

g_r is the geometry efficiency for random events, considered the same as g_t^2 .

The Noise Equivalent Count Rate (NECR) is the number of counts detected as a function of the activity concentration, after correcting the effects of random and scatter events taking into account dead-time losses. It is a standard measure of signal to noise in reconstructed PET images.

	gamma interaction	gamma direct	gamma diffused	readout grains	diffused impact
20 μ m:	420282	319732	100550	170804	26024
16 μ m:	420282	319732	100550	98587	8324

Table 1
History of 1000000 single photon events

$$NECR = True^2 / (True + Scatter + k.Random)$$

where

k is a correction factor for random coincidences (k=1 or 2).

To illuminate the possibilities of SSG HDM PET two different grains suspensions and corresponding electronic tuning are considered: the first one with 10 μ m radius tin grains and with an electronic threshold corresponding to the magnetic flux penetration in one grain, the second with 8 μ m radius tin grains. We presume working at a temperature (between 200 and 500 mK) allowing a ΔH_{max} of 5 eV. With an electronic threshold corresponding to two simultaneously flipping grains, the performance for each situation is given below for 10⁶ events, by the following numbers presented in Table 2:

If we suppress the phantom and the depth of the vessel, we get 384990 gamma's directly in our system. Of these 384990, 367770 are on the 511keV as entry energy. In the system with phantom and vessel, we get 267670 photons with 511 keV. But, in reality, a large fraction of photons give a signal in the same angle as the direct photons. We consider the threshold angle for diffused gammas as 0.234 radians.

The probability of escape P can be evaluated to 0.7281.

The probability of direct impact is 0.8793.

The solid angle of our system is for 20 cm of length of the detector and 5 cm of radius:

$$4\pi(1 - \cos(\arctan(0.5)))$$

$$= 4\pi(1 - \frac{2}{\sqrt{5}})$$

and

$$g_r = \frac{2}{\sqrt{5}} = 0.9$$

ϵ is the product of the materialisation factor by the electronic efficiency which is given by Table 2.

radius	true	diffused	scatter fraction
10 μm	170804/319732 0.534	26024/100550 0.26	26024/170804 0.1523
8 μm	98587/319732 0.380	8324/100550 0.083	8324/98587 0.08443

Table 2

Photon electronic efficiency

The gamma materialization factor is

$$m = 0.367770/0.9=0.419$$

This gives:

$$\text{For a radius of } 10 \mu\text{m}, \epsilon = 0.419 \cdot 0.534 = 0.2036$$

$$\text{For a radius of } 8 \mu\text{m}, \epsilon = 0.419 \cdot 0.380 = 0.1520$$

This allows us to estimate the

$$NECR = True \frac{1}{1 + f_s + 2\rho \cdot g_t \cdot \tau}$$

with:

$$\tau = 10^{-8}, g_t = 0.9, P = 0.7281$$

and:

$$True = \rho \cdot \epsilon^2 \cdot g_t \cdot P^2$$

The maximum acquisition rate is of 10^8 , this gives, for a source of 10^8 like the one cited in reference [8]:

For 10 μm radius,

$$\epsilon = 0.2036, True = 1.9810^6$$

$$NECR = \frac{0.019810^8}{1.1523 + \rho 1.8 \cdot 10^{-8}} = 0.66 \cdot 10^6$$

For 8 μm radius,

$$\epsilon = 0.1520, True = 9.10^5$$

$$NECR = \frac{0.00910^8}{1.08443 + \rho 1.8 \cdot 10^{-8}} = 0.3 \cdot 10^6$$

radius	10^8	10^7	10^6
10 μm	666000 33%	150000 75%	17500 82%
8 μm	300000 30%	71000 80%	8200 90%

Table 3

NECR according to the intensity of the source (10^6 , 10^7 and 10^8 Becquerel), and to the radius of the grains, given in counts per second and percentage of the whole counting rate.

The number of diffused, *Scatter*, is $3 \cdot 10^5$ and $0.7 \cdot 10^5$ respectively in these two cases.

The number of random coincidences, *Random*, is the most important noise: with such a source of 10^8 , and a window of 10 nanosecond, we get $0.9 \cdot 10^6$ and $0.54 \cdot 10^6$ respective of noise.

Improvement of the NECR can be achieved by following paths:

The g_t factor can be increased by a new geometry covering a larger solid angle.

The NECR is proportional to the square of the materialization factor: with three sheets of detecting rows, we should get an electronic efficiency of 0.784 instead of 0.4, this implies a multiplication of the NECR of about 4: this should give:

NECR= $2.6 \cdot 10^6$ for 10 μm radius, and NECR= $1.2 \cdot 10^6$ for 8 μm radius. Noise reduction is improved with sharper time coincidences: we take 10^{-8} second.

Increasing electronic efficiency can be achieved in more sophisticated reconstruction taking into account when two cells give a signal.

In usual case, sources of lower intensity are used, in this case we get a more efficient NECR (Table 3, for 1 sheet of row):

5 Conclusions:

SSG PET is an alternative to classical techniques pushed to their limits. As often is the case the flexibility of a new solution is repaid by the familiarity with new techniques, in this case very low temperature cryogenics which have made significant progress toward simplicity and an easy-to-use operation, in the last ten years. Low temperature and superconductors are already used for medical

imaging (MRI magnets). We would underline the fact that SSG PET has no optical component and no crystal detector. As a result it is open to various designs in spite of the fact that it must operate at a low temperature. Secondly: individual pixels at the actual stage of electronics allow high counting rates. Thirdly : SSG allows energy selection without any numerical treatment : the monitoring of the magnetic field is enough. Although this paper deals with the feasibility of PET systems for small animals we would like also stress that the non crystalline nature of the detector allows the realization of pixels with a volumic fraction at their input in a low density matrix. In that case the detector is mostly sensitive to soft X ray (in fact it was most often used in that range of energy). Therefore a combined PET+CT system with the same geometry and electronics is perfectly feasible.

6 Acknowledgments

We would like to thank MM Bonnierbale for his technical help. We would like to thank M Lallemand, Director of ASCI (Application Scientifique du Calcul Intensif), for his support and help with the numerical simulations.

References

- [1] G. Waysand and al. Experimental study of dielectric and diamagnetic properties of dispersions of tin superconducting microspheres. *Superconducting and Low-Temperature Particle Detectors, Elsevier Science Publishers B.V. (North Holland)*, pages 201–215, 1989.
- [2] R. Bruère Dawson et al. Conventional readout electronics for superheated superconducting grains, first experimental results. *Nuclear Instruments and Methods in Physics Research*, pages 211–216, 1989.
- [3] CERN. *GEANT Users Manual*.
- [4] H. Dubois. *Rupture de la surchauffe supraconductrice dans des suspensions de microsphères d'étain à très basse température*. PhD thesis, Université Paris VI, 1996.
- [5] U.Geigenmüller. On dispersion of superheated superconducting spheres. *Journal de Physique*, page 405, 1988.
- [6] U.Geigenmüller and P.Mazur. Many body hydrodynamic interactions between spherical drops in an emulsion. *PHYSICA*, pages 269–298, 1986.
- [7] A. Penaranda and al. Diamagnetic interactions in disordered suspensions of metastable superconducting granules. *European Physical Journal B*, pages 155–165, 2002.

- [8] J.S. Huber and W.W. Moses. Conceptual design of a high sensitivity small animal pet camera with 4π coverage. *IEEE Trans. Nuc. Science*, page 498, 1999.